ESPRIT-TYPE ALGORITHMS FOR A RECEIVED MIXTURE OF CIRCULAR AND STRICTLY NON-CIRCULAR SIGNALS

Jens Steinwandt [1], *Florian Roemer* [2], *and Martin Haardt* [1]

[1] Communications Research Laboratory, Ilmenau University of Technology, P.O. Box 100565, 98684 Ilmenau, Germany
[2] Digital Broadcasting Research Laboratory, Ilmenau University of Technology, P.O. Box 100565, 98684 Ilmenau, Germany
{jens.steinwandt, florian.roemer, martin.haardt}@tu-ilmenau.de, www.tu-ilmenau.de/crl

ABSTRACT

Recently, ESPRIT-based parameter estimation algorithms have been developed to exploit the structure of signals from strictly second-order (SO) non-circular (NC) sources. They achieve a higher estimation accuracy and can resolve up to twice as many sources. However, these NC methods assume that all the received signals are strictly non-circular. In this paper, we present the C-NC Standard ESPRIT and the C-NC Unitary ESPRIT algorithms designed for the more practical scenario of a received mixture of circular and strictly non-circular signals. Assuming that the number of circular and strictly non-circular signals is known, the two proposed methods yield closed-form estimates and C-NC Unitary ESPRIT also enables an entirely real-valued implementation. As a main result, it is shown that the estimation accuracy of the presented algorithms improves with an increasing number of strictly non-circular signals among a fixed number of sources. Thereby, not only the estimation accuracy of the strictly non-circular signals themselves is improved, but also the estimation accuracy of the circular signals. These results are validated by simulations.

Index Terms— ESPRIT, non-circular sources, mixture, DOA estimation.

1. INTRODUCTION

Estimating the directions of arrival (DOA) of signals captured by a sensor array has long been of great research interest, given its importance in a broad variety of applications such as radar, sonar, and wireless communications. Among various subspace-based parameter estimation schemes, ESPRIT-type algorithms [1], [2] are some of the most powerful estimators due to their high-resolution capabilities and their low complexity as they provide closed-form estimates. However, these traditional methods do not take advantage of the potential structure of the received signals such as their second-order (SO) non-circularity.

Recently, a number of improved subspace-based parameter estimation schemes such as NC MUSIC [3], NC Root-MUSIC [4], NC Standard ESPRIT [5], and NC Unitary ESPRIT [6], [7] have been developed. They efficiently exploit prior knowledge on the structure of the incident signals from strictly SO non-circular (NC) sources [8]. Important examples of digital modulation schemes that use such signals are BPSK, PAM, Offset-QPSK, and ASK among others. It has been shown that taking the signals' strict SO non-circularity into account provides a significant reduction in the estimation error and doubles the number of resolvable sources [7].

This work was supported by the International Graduate School on Mobile Communications (MOBICOM), Ilmenau, Germany.

The aforementioned NC algorithms heavily rely on the assumption that all the impinging signals are strictly non-circular. Therefore, they cannot deal with the more realistic scenario of a received mixture of circular and strictly non-circular signals. In order to cope with this more general scenario, the two methods [9] and [10] based on the spectral MUSIC algorithm have been designed. They estimate the DOAs of the circular and non-circular signals jointly [9] or separately [10] and improve the estimation accuracy while increasing the number of detectable signals. Another MUSIC-based method for arbitrary non-circular sources has been developed in [11]. However, all these algorithms require a computationally expensive peak search of the obtained MUSIC pseudo spectrum. Therefore, it is highly desirable to devise ESPRIT-based algorithms for the scenario of interest that provide closed-form estimates.

In this paper, we present the C-NC Standard ESPRIT and the C-NC Unitary ESPRIT algorithms designed for the practical scenario of coexisting circular and strictly non-circular signals. We assume that the number of circular and strictly non-circular sources is known. Otherwise, they can be estimated using, e.g., the method from [12]. The two proposed methods yield closed-form estimates and C-NC Unitary ESPRIT also enables an entirely real-valued implementation. It is shown that each circular signal can be decomposed into two independent virtual strictly non-circular signals with the same direction. Thus, we obtain two parameter estimates for each circular source that are subsequently combined in a suitable way, e.g., by computing the average. Moreover, as a main result it is observed via simulations that the performance of the proposed algorithms improves when the number of strictly non-circular signals among a fixed number of sources increases. Interestingly, apart from the better estimation accuracy for the strictly non-circular signals themselves, it is shown that the presence of only a single strictly non-circular source already improves the estimation accuracy of the circular signals. This is due to the suitable combination of the two corresponding estimates for each circular source, which improves their estimation accuracy. All our observations are verified by simulation results.

2. DATA MODEL

Suppose that an arbitrarily formed shift-invariant-structured sensor array [1], [2], i.e., it can be divided into two identical displaced subarrays, composed of M isotropic elements receives uncorrelated narrowband signals from d far-field sources. The N subsequent data snapshots can be modeled as

$$\boldsymbol{X} = \boldsymbol{A}\boldsymbol{S} + \boldsymbol{N} \in \mathbb{C}^{M \times N}, \tag{1}$$

where the array steering matrix $\boldsymbol{A} = [\boldsymbol{a}(\mu_1), \ldots, \boldsymbol{a}(\mu_d)] \in \mathbb{C}^{M \times d}$ contains the array steering vectors $\boldsymbol{a}(\mu_i)$ corresponding to the i-th

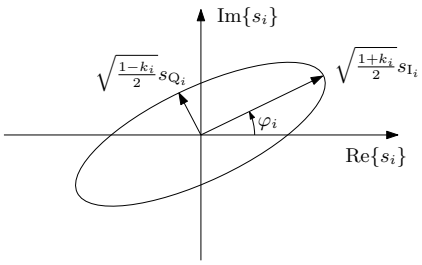

Fig. 1. Model for arbitrary non-circular signals.

spatial frequency μ_i with $i = 1, \ldots, d$, $\boldsymbol{S} \in \mathbb{C}^{d\times N}$ represents the source symbol matrix, and $\boldsymbol{N} \in \mathbb{C}^{M\times N}$ consists of the additive sensor noise samples.

Applying ESPRIT-type algorithms for the parameter estimation, we use the shift-invariance of $\boldsymbol{A}$, i.e.,

$$\boldsymbol{J}_1\boldsymbol{A}\boldsymbol{\Phi} = \boldsymbol{J}_2\boldsymbol{A}, \tag{2}$$

where $\boldsymbol{J}_1$ and $\boldsymbol{J}_2 \in \mathbb{R}^{M^{(\mathrm{sel})}\times M}$ are the selection matrices that select $M^{(\mathrm{sel})}$ out of M sensors for each of the two subarrays and $\boldsymbol{\Phi} = \mathrm{diag}\{[\mathrm{e}^{\mathrm{j}\mu_1}, \ldots, \mathrm{e}^{\mathrm{j}\mu_d}]\} \in \mathbb{C}^{d\times d}$ contains the desired spatial frequencies.

2.1. Source Model

In this section, we introduce a new model to describe signal sources with arbitrary SO non-circularity. The advantage of this model is that any digital modulation scheme can be represented. As illustrated in Fig. 1, the i-th received signal can be modeled in the complex plane as follows:

$$s_i = \mathrm{e}^{\mathrm{j}\varphi_i}\left(\sqrt{\frac{1+k_i}{2}}s_{\mathrm{I}_i} + \mathrm{j}\sqrt{\frac{1-k_i}{2}}s_{\mathrm{Q}_i}\right),\ i = 1, \ldots, d, \tag{3}$$

where φ_i is the rotation phase, k_i with $0 \le k_i \le 1$ is the magnitude of the non-circularity coefficient, and s_{I_i} and s_{Q_i} represent the in-phase and quadrature components of the complex signal s_i, respectively. Geometrically, the model in (3) describes an ellipse centered at the origin, which is rotated by φ_i and where the axes are parameterized by k_i. The parameterization in k_i is chosen such that $\mathbb{E}\{|s_{\mathrm{I}_i}|^2\} = 1$ for $\mathbb{E}\{|s_{\mathrm{I}_i}|^2\} = 1$ and $\mathbb{E}\{|s_{\mathrm{Q}_i}|^2\} = 1$, and $\mathbb{E}\{s_i^2\} = \mathrm{e}^{\mathrm{j}2\varphi_i}(k_i + \mathrm{j}\sqrt{1-k_i^2}\cdot\mathbb{E}\{s_{\mathrm{I}_i}s_{\mathrm{Q}_i}\})$. If s_{I_i} and s_{Q_i} are uncorrelated, which is often the case for linear digital modulation schemes, we have $\mathbb{E}\{s_{\mathrm{I}_i}s_{\mathrm{Q}_i}\} = 0$ and therefore $\mathbb{E}\{s_i^2\} = k_i\mathrm{e}^{\mathrm{j}2\varphi_i}$. Thus, the complex non-circularity coefficient defined in [8] is given by

$$\rho_i = \frac{\mathbb{E}\{s_i^2\}}{\mathbb{E}\{|s_i|^2\}} = |\rho_i|\mathrm{e}^{\mathrm{j}\psi_i} = k_i\mathrm{e}^{\mathrm{j}2\varphi_i}, \tag{4}$$

where $|\rho_i| = k_i$ and the non-circularity phase is $\psi_i = 2\varphi_i$. Note that the case $k_i = 0$ represents a circular source, where the rotation phase φ_i is irrelevant as well as undetermined. The case $k_i = 1$ represents a strictly non-circular (rectilinear) source, i.e., $s_i = \mathrm{e}^{\mathrm{j}\varphi_i}s_{0_i}$ with $s_{0_i} = s_{\mathrm{I}_i}$. Thus, the complex symbol amplitudes of each rectilinear source lie on a rotated line in the complex plane [7]. In what follows, we will focus on a received mixture of circular ($k_i = 0$) and strictly non-circular sources ($k_i = 1$) as this case is very relevant in practical scenarios.

Let us denote the number of strictly non-circular sources and the number of circular sources as $d^{(\mathrm{nc})}$ and $d^{(\mathrm{c})}$ respectively, where $d^{(\mathrm{nc})} + d^{(\mathrm{c})} = d$. Collecting the d signals into the matrix $\boldsymbol{S}$, we let the first $d^{(\mathrm{nc})}$ rows in $\boldsymbol{S}$ represent the strictly non-circular signals without loss of generality. Then, similarly to [11], we virtually decompose each of the circular sources into two uncorrelated strictly non-circular sources with the same DOA. We obtain

$$\boldsymbol{S} = \begin{bmatrix}(\boldsymbol{\Psi}_1\boldsymbol{S}_0)^{\mathrm{T}} & \left(\begin{bmatrix}\boldsymbol{I}_{d^{(\mathrm{c})}} & \mathrm{j}\boldsymbol{I}_{d^{(\mathrm{c})}}\end{bmatrix}\begin{bmatrix}\boldsymbol{S}_{\mathrm{I}}\\ \boldsymbol{S}_{\mathrm{Q}}\end{bmatrix}\right)^{\mathrm{T}}\end{bmatrix}^{\mathrm{T}} \tag{5}$$

$$= \begin{bmatrix}\boldsymbol{\Psi}_1 & \boldsymbol{0}\\ \boldsymbol{0} & \begin{bmatrix}\boldsymbol{I}_{d^{(\mathrm{c})}} & \mathrm{j}\boldsymbol{I}_{d^{(\mathrm{c})}}\end{bmatrix}\end{bmatrix}\begin{bmatrix}\boldsymbol{S}_0\\ \boldsymbol{S}_{\mathrm{I}}\\ \boldsymbol{S}_{\mathrm{Q}}\end{bmatrix} = \boldsymbol{\Psi}\tilde{\boldsymbol{S}}, \tag{6}$$

where $\boldsymbol{\Psi}_1 = \mathrm{diag}\{\mathrm{e}^{\mathrm{j}\varphi_k}\}_{k=1}^{d^{(\mathrm{nc})}}$ represents the rotation phases corresponding to the strictly non-circular sources. Furthermore, we have $\boldsymbol{\Psi} \in \mathbb{C}^{d\times\tilde{d}}$ with $\tilde{d} = d^{(\mathrm{nc})} + 2d^{(\mathrm{c})}$ and the real-valued matrix $\tilde{\boldsymbol{S}} \in \mathbb{R}^{\tilde{d}\times N}$ contains the symbols of the strictly non-circular sources $\boldsymbol{S}_0 \in \mathbb{R}^{d^{(\mathrm{nc})}\times N}$ as well as the real and imaginary parts of the circular signals $\boldsymbol{S}_{\mathrm{I}} \in \mathbb{R}^{d^{(\mathrm{c})}\times N}$ and $\boldsymbol{S}_{\mathrm{Q}} \in \mathbb{R}^{d^{(\mathrm{c})}\times N}$, respectively.

Using (6), the model (1) can be equivalently expressed as

$$\boldsymbol{X} = \boldsymbol{A}\boldsymbol{\Psi}\tilde{\boldsymbol{S}} + \boldsymbol{N} = \tilde{\boldsymbol{A}}\tilde{\boldsymbol{S}} + \boldsymbol{N}, \tag{7}$$

where $\tilde{\boldsymbol{A}} = \boldsymbol{A}\boldsymbol{\Psi} \in \mathbb{C}^{M\times\tilde{d}}$ is the modified array steering matrix. The new column dimensions of $\tilde{\boldsymbol{A}}$ again indicate the virtual decomposition of the circular sources.

2.2. Modified Array Model

In order to take advantage of the strict non-circularity of the $d^{(\mathrm{nc})}$ sources and the virtual strict non-circularity of the circular sources, we apply a preprocessing scheme to (7) and define the augmented measurement matrix $\boldsymbol{X}^{(\mathrm{nc})} \in \mathbb{C}^{2M\times N}$ similarly to [6], [7] as

$$\boldsymbol{X}^{(\mathrm{nc})} = \begin{bmatrix}\boldsymbol{X}\\ \boldsymbol{\Pi}_M\boldsymbol{X}^*\end{bmatrix} = \begin{bmatrix}\tilde{\boldsymbol{A}}\\ \boldsymbol{\Pi}_M\tilde{\boldsymbol{A}}^*\end{bmatrix}\tilde{\boldsymbol{S}} + \begin{bmatrix}\boldsymbol{N}\\ \boldsymbol{\Pi}_M\boldsymbol{N}^*\end{bmatrix} \tag{8}$$

$$= \boldsymbol{A}^{(\mathrm{nc})}\tilde{\boldsymbol{S}} + \boldsymbol{N}^{(\mathrm{nc})}. \tag{9}$$

where $\tilde{\boldsymbol{S}}$ is real-valued, $\boldsymbol{A}^{(\mathrm{nc})} \in \mathbb{C}^{2M\times\tilde{d}}$ is the virtual steering matrix, and $\boldsymbol{\Pi}_M$ is the $M \times M$ exchange matrix with ones on its antidiagonal and zeros elsewhere. Next, we rewrite the physical array steering matrix $\boldsymbol{A}$ and let its first $d^{(\mathrm{nc})}$ columns represent the strictly non-circular sources. We have

$$\boldsymbol{A} = \left[\boldsymbol{a}(\mu_1), \ldots, \boldsymbol{a}(\mu_{d^{(\mathrm{nc})}}), \boldsymbol{a}(\mu_{d^{(\mathrm{nc})}+1}), \ldots, \boldsymbol{a}(\mu_d)\right] \tag{10}$$

$$= \begin{bmatrix}\boldsymbol{A}_1 & \boldsymbol{A}_2\end{bmatrix}. \tag{11}$$

Using (11), the matrix $\boldsymbol{A}^{(\mathrm{nc})}$ can be expressed as

$$\boldsymbol{A}^{(\mathrm{nc})} = \begin{bmatrix}\boldsymbol{A}_1\boldsymbol{\Psi}_1 & \boldsymbol{A}_2\begin{bmatrix}\boldsymbol{I}_d & \mathrm{j}\boldsymbol{I}_d\end{bmatrix}\\ \boldsymbol{\Pi}_M\boldsymbol{A}_1^*\boldsymbol{\Psi}_1^* & \boldsymbol{\Pi}_M\boldsymbol{A}_2^*\begin{bmatrix}\boldsymbol{I}_d & -\mathrm{j}\boldsymbol{I}_d\end{bmatrix}\end{bmatrix}. \tag{12}$$

It is evident from (12) that after the decomposition of the circular sources, the steering vectors corresponding to the virtual strictly non-circular sources are orthogonal to each other. Furthermore, the extended row dimension of $\boldsymbol{A}^{(\mathrm{nc})} \in \mathbb{C}^{2M\times\tilde{d}}$ can be interpreted as a virtual doubling of the sensor elements, which implies that at most up to $2M^{(\mathrm{sel})}$ sources can be resolved. In the special case of a uniform linear array (ULA) with maximum overlap, we have $M^{(\mathrm{sel})} = M - 1$. Then, assuming that the $\tilde{d}$ sources are distinct,

$\boldsymbol{A}^{(\mathrm{nc})}$ has a full column rank of $\tilde{d}$. Therefore, the maximum number of resolvable sources must fulfill

$$\tilde{d} = d^{(\mathrm{nc})} + 2d^{(\mathrm{c})} \leq 2M^{(\mathrm{sel})}. \tag{13}$$

Hence, rewriting (13) as $d = d^{(\mathrm{nc})} + d^{(\mathrm{c})} \leq M^{(\mathrm{sel})} + d^{(\mathrm{nc})}/2$, it is apparent that if at least two strictly non-circular sources are among the sources, more than the traditional limit of $M^{(\mathrm{sel})}$ sources ($M-1$ sources for a ULA) can be identified.

Remark 1: If all the sources are strictly non-circular, i.e., $d^{(\mathrm{c})} = 0$, the model in (9) reduces to

$$\boldsymbol{X}^{(\mathrm{nc})} = \begin{bmatrix} \boldsymbol{A} \\ \boldsymbol{\Pi}_M \boldsymbol{A}^* \boldsymbol{\Psi}^* \boldsymbol{\Psi}^* \end{bmatrix} \boldsymbol{S} + \boldsymbol{N}^{(\mathrm{nc})}, \tag{14}$$

with $\boldsymbol{A}^{(\mathrm{nc})} \in \mathbb{C}^{2M \times d}$, $\boldsymbol{A} = \boldsymbol{A}_1, \boldsymbol{\Psi} = \boldsymbol{\Psi}_1, \tilde{\boldsymbol{S}} = \boldsymbol{S}_0$, and where we used the property $\boldsymbol{S}_0 = \boldsymbol{\Psi}^* \boldsymbol{S}$. This case was considered in [7]. There, it was shown that the number of resolvable sources is doubled, i.e., $d^{(\mathrm{nc})} \leq 2M^{(\mathrm{sel})}$ and the estimation error is significantly reduced compared to the conventional ESPRIT algorithm [1], which does not exploit the NC structure of the signals.

Remark 2: If all the sources are circular, i.e., $d^{(\mathrm{nc})} = 0$, the model in (9) simplifies to

$$\boldsymbol{X}^{(\mathrm{nc})} = \begin{bmatrix} \boldsymbol{A} \begin{bmatrix} \boldsymbol{I}_d & \mathrm{j}\boldsymbol{I}_d \end{bmatrix} \\ \boldsymbol{\Pi}_M \boldsymbol{A}^* \begin{bmatrix} \boldsymbol{I}_d & -\mathrm{j}\boldsymbol{I}_d \end{bmatrix} \end{bmatrix} \begin{bmatrix} \boldsymbol{S}_{\mathrm{I}} \\ \boldsymbol{S}_{\mathrm{Q}} \end{bmatrix} + \boldsymbol{N}^{(\mathrm{nc})}, \tag{15}$$

where $\boldsymbol{A} = \boldsymbol{A}_2$. In this case, the preprocessing in (8) does not yield a performance improvement compared to the conventional ESPRIT algorithm [1], which will be shown in Section 4. Therefore, (15) corresponds to the conventional ESPRIT algorithm.

As a next step, it is straightforward to see that if $\boldsymbol{A}$ is shift-invariant, i.e., equation (2) is fulfilled, so is $\tilde{\boldsymbol{A}}$, such that $\boldsymbol{J}_1 \tilde{\boldsymbol{A}} \boldsymbol{\Gamma} = \boldsymbol{J}_2 \tilde{\boldsymbol{A}}$ holds, where the diagonal matrix $\boldsymbol{\Gamma} \in \mathbb{C}^{\tilde{d} \times \tilde{d}}$ contains the $\tilde{d}$ spatial frequencies. We emphasize again that the $d^{(\mathrm{c})}$ circular sources are represented by two strictly non-circular sources each and therefore their corresponding spatial frequencies occur twice.

Similarly to [7], it can be shown that in this case, the augmented array steering matrix $\boldsymbol{A}^{(\mathrm{nc})}$ also possesses the shift-invariance structure so that

$$\boldsymbol{J}_1^{(\mathrm{nc})} \boldsymbol{A}^{(\mathrm{nc})} \boldsymbol{\Gamma} = \boldsymbol{J}_2^{(\mathrm{nc})} \boldsymbol{A}^{(\mathrm{nc})}, \tag{16}$$

where the $(2M^{(\mathrm{sel})} \times 2M)$-dimensional selection matrices in the NC case are defined by

$$\boldsymbol{J}_1^{(\mathrm{nc})} = \begin{bmatrix} \boldsymbol{J}_1 & \boldsymbol{0} \\ \boldsymbol{0} & \boldsymbol{\Pi}_M^{(\mathrm{sel})} \boldsymbol{J}_2 \boldsymbol{\Pi}_M \end{bmatrix}, \quad \boldsymbol{J}_2^{(\mathrm{nc})} = \begin{bmatrix} \boldsymbol{J}_2 & \boldsymbol{0} \\ \boldsymbol{0} & \boldsymbol{\Pi}_M^{(\mathrm{sel})} \boldsymbol{J}_1 \boldsymbol{\Pi}_M \end{bmatrix}.$$

3. PROPOSED ESPRIT-TYPE ALGORITHMS

In this section, we derive the proposed C-NC Standard ESPRIT and C-NC Unitary ESPRIT methods that are designed for the coexistence of circular and strictly non-circular signals. They are based on the data model (9).

3.1. C-NC Standard ESPRIT Algorithm

Based on the noisy augmented data model (9), the augmented signal subspace $\hat{\boldsymbol{U}}_{\mathrm{s}}^{(\mathrm{nc})} \in \mathbb{C}^{2M \times \tilde{d}}$ is estimated by computing the $\tilde{d}$ dominant left singular vectors of $\boldsymbol{X}^{(\mathrm{nc})}$. As $\boldsymbol{A}^{(\mathrm{nc})}$ and $\hat{\boldsymbol{U}}_{\mathrm{s}}^{(\mathrm{nc})}$ span approximately the same column space, a non-singular matrix $\boldsymbol{T} \in \mathbb{C}^{\tilde{d} \times \tilde{d}}$ can be found such that $\boldsymbol{A}^{(\mathrm{nc})} \approx \hat{\boldsymbol{U}}_{\mathrm{s}}^{(\mathrm{nc})} \boldsymbol{T}$. Using this relation, the augmented shift invariance equation can be expressed as

$$\boldsymbol{J}_1^{(\mathrm{nc})} \hat{\boldsymbol{U}}_{\mathrm{s}}^{(\mathrm{nc})} \boldsymbol{\Upsilon} \approx \boldsymbol{J}_2^{(\mathrm{nc})} \hat{\boldsymbol{U}}_{\mathrm{s}}^{(\mathrm{nc})}, \tag{17}$$

where $\boldsymbol{\Upsilon} \approx \boldsymbol{T}\boldsymbol{\Gamma}\boldsymbol{T}^{-1}$. The unknown matrix $\boldsymbol{\Upsilon} \in \mathbb{C}^{\tilde{d} \times \tilde{d}}$ can be estimated by means of a suitable least squares (LS) method [13]. The simple LS solution for instance is given by

$$\hat{\boldsymbol{\Upsilon}} = \left(\boldsymbol{J}_1^{(\mathrm{nc})} \hat{\boldsymbol{U}}_{\mathrm{s}}^{(\mathrm{nc})} \right)^{+} \boldsymbol{J}_2^{(\mathrm{nc})} \hat{\boldsymbol{U}}_{\mathrm{s}}^{(\mathrm{nc})}, \tag{18}$$

where $(\cdot)^+$ stands for the Moore-Penrose pseudo inverse. Finally, the desired $\tilde{d}$ spatial frequency estimates are extracted by $\hat{\mu}_i = \arg\{\hat{\lambda}_i\}$, $i = 1, \ldots, \tilde{d}$, where $\hat{\lambda}_i$ are the eigenvalues of $\hat{\boldsymbol{\Upsilon}}$.

Note that due to the decomposition of the circular sources into two strictly non-circular sources each, we obtain $\tilde{d} = d^{(\mathrm{nc})} + 2d^{(\mathrm{c})}$ spatial frequency estimates, while only $d = d^{(\mathrm{nc})} + d^{(\mathrm{c})}$ actual sources are present. Thus, the two correctly paired estimates obtained for each circular source can be combined in a suitable manner. As both estimates are equally reliable, we simply choose the average according to

$$\hat{\mu}_n = \frac{1}{2} \left(\hat{\mu}_n^{(1)} + \hat{\mu}_n^{(2)} \right), \quad n = 1, \ldots, d^{(\mathrm{c})}. \tag{19}$$

In order to compute the mean in (19), we need to discriminate the estimates associated with the circular sources from those for the strictly non-circular sources. As the numbers $d^{(\mathrm{nc})}$ and $d^{(\mathrm{c})}$ are assumed known, the pairs of estimates for each circular source can be identified by taking the $d^{(\mathrm{c})}$ pairs of two estimates that are closest to each other among all the estimates.

3.2. C-NC Unitary ESPRIT Algorithm

In addition to the shift-invariance, the traditional Unitary ESPRIT algorithm requires the sensor array to be centro-symmetric, and it includes forward-backward-averaging (FBA) as well as the transformation into the real-valued domain as preprocessing steps [2]. However, after the initial preprocessing for non-circular sources in (8), it can be shown in analogy to [7] that the augmented array steering matrix $\boldsymbol{A}^{(\mathrm{nc})}$ in (12) always exhibits centro-symmetry even if the physical array is not centro-symmetric. Hence, the proposed C-NC Unitary ESPRIT algorithm is applicable to a broader variety of array geometries.

As proven in [7], the real-valued matrix after applying FBA and the real-valued transformation to the NC measurement matrix $\boldsymbol{X}^{(\mathrm{nc})}$ is given by

$$\varphi(\boldsymbol{X}^{(\mathrm{nc})}) = 2 \cdot \begin{bmatrix} \mathrm{Re}\{\boldsymbol{X}\} & \boldsymbol{0} \\ \mathrm{Im}\{\boldsymbol{X}\} & \boldsymbol{0} \end{bmatrix}. \tag{20}$$

Next, we compute the $\tilde{d}$ dominant left singular vectors $\hat{\boldsymbol{E}}_{\mathrm{s}}^{(\mathrm{nc})} \in \mathbb{R}^{2M \times \tilde{d}}$ through a real-valued SVD of $\varphi(\boldsymbol{X}^{(\mathrm{nc})})$, where the factor 2 and the zero columns can be omitted. Defining the transformed selection matrices $\boldsymbol{K}_1^{(\mathrm{nc})}$ and $\boldsymbol{K}_2^{(\mathrm{nc})}$ according to [7], the real-valued shift-invariance equation

$$\boldsymbol{K}_1^{(\mathrm{nc})} \hat{\boldsymbol{E}}_{\mathrm{s}}^{(\mathrm{nc})} \boldsymbol{\Omega} \approx \boldsymbol{K}_2^{(\mathrm{nc})} \hat{\boldsymbol{E}}_{\mathrm{s}}^{(\mathrm{nc})} \tag{21}$$

can be solved for $\boldsymbol{\Omega} \in \mathbb{R}^{\tilde{d} \times \tilde{d}}$ using, for instance, LS. Finally, the $\tilde{d}$ spatial frequencies are extracted via $\hat{\mu}_i = 2 \cdot \arctan(\hat{\omega}_i)$, $i = 1, \ldots, \tilde{d}$ from the real-valued eigenvalues $\hat{\omega}_i$ of $\hat{\boldsymbol{\Omega}}$.

The pairing of the two estimates for each circular source and the subsequent averaging are performed in the same way as described in the previous section for C-NC Standard ESPRIT.

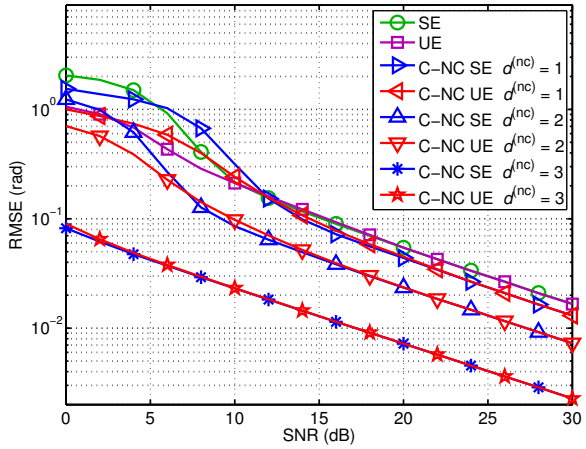

Fig. 2. RMSE versus SNR for $M = 8$, $N = 100$, and $d = 4$ uncorrelated sources at $\boldsymbol{\mu} = [0, 0.5, 0.8, 1.2]$ with varying $d^{(\mathrm{nc})}$.

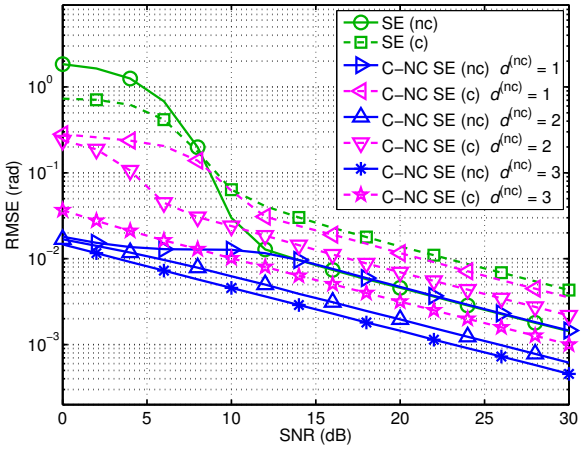

Fig. 3. RMSE versus SNR for the strictly non-circular "(nc)" source at $\mu_1 = 0$ and the circular "(c)" source at $\mu_4 = 1.2$ for $M = 8$, $N = 100$, $P^{(\mathrm{nc})} = 5$, and $P^{(\mathrm{c})} = 1$ with varying $d^{(\mathrm{nc})}$.

4. SIMULATION RESULTS

In this section, we provide simulation results to assess the performance of the presented C-NC Standard ESPRIT (C-NC SE) and C-NC Unitary ESPRIT (C-NC UE) algorithms designed for the mixture of circular and strictly non-circular sources. We compare the proposed methods to the traditional ESPRIT-type methods (SE/UE) [1], [2] that do not exploit the NC structure of the strictly non-circular signals. A uniform linear array (ULA) with $M = 8$ isotropic elements spaced $\delta = \lambda/2$ apart is used. The circular signals are QPSK signals and the real-valued strictly non-circular signals are BPSK-modulated signals. Moreover, we assume circularly symmetric white Gaussian sensor noise. The results are obtained by averaging over 5000 Monte Carlo runs.

In the first experiment, we assume that $d = 4$ uncorrelated sources with unit power impinge on the array with the spatial frequencies $\boldsymbol{\mu} = [0, 0.5, 0.8, 1.2]$. We vary the number of strictly non-circular sources and start from $d^{(\mathrm{nc})} = 1$ associated with μ_1 up to $d^{(\mathrm{nc})} = 3$ by adding more elements of $\boldsymbol{\mu} = [0, 0.5, 0.8, 1.2]$ from the left. The rotation phases of the strictly non-circular sources are separated by $\pi/4$ starting from 0. The number of snapshots is $N = 100$. Fig. 2 illustrates the total RMSE as a function of the SNR. It can be seen that the proposed algorithms outperform SE and UE whenever strictly non-circular sources are present. Moreover, their performance improves when $d^{(\mathrm{nc})}$ increases.

In Fig. 3, we use the same scenario but display the RMSE of C-NC SE versus the SNR for the strictly non-circular "(nc)" source at $\mu_1 = 0$ and the circular "(c)" source at $\mu_d = 1.2$ under the variation from $d^{(\mathrm{nc})} = 1$ to $d^{(\mathrm{nc})} = 3$. All the strictly non-circular sources and the circular sources have the signal powers $P^{(\mathrm{nc})} = 5$ and $P^{(\mathrm{c})} = 1$, respectively. Interestingly, an increasing number of $d^{(\mathrm{nc})}$ not only improves the estimation accuracy of the strictly non-circular source, but also that of the circular source.

In the second experiment, we analyze the performance as a function of the DOA separation compared to SE and UE. We assume $d = 2$ uncorrelated sources, where we have a strictly non-circular "(nc)" source located at $\mu_1 = -1$ and a circular "(c)" source at $\mu_2 = -1 + \mathrm{sep}$. The source powers are $P^{(\mathrm{nc})} = 1$ and $P^{(\mathrm{c})} = 2$. Moreover, the rotation phase of the strictly non-circular source is $\varphi_1 = \pi/8$ and $N = 100$. Fig. 4 depicts the RMSE of C-NC SE versus the separation. It is evident that in general, the performance improves when the separation grows. More importantly, the improvement in the estimation accuracy of the circular source due to the presence of the strictly non-circular source is shown. This gain is largest for closely-spaced sources and vanishes if the sources are further apart.

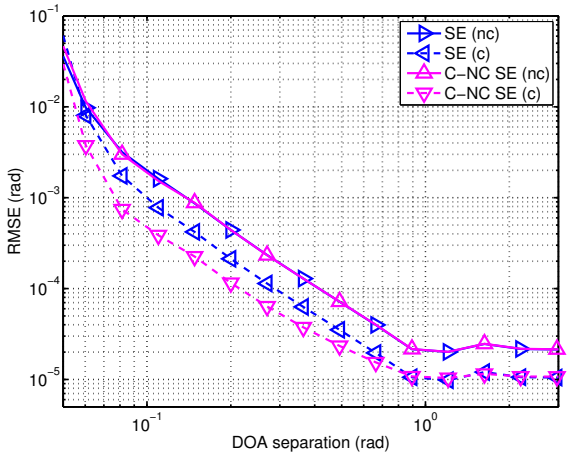

Fig. 4. RMSE versus the DOA separation "(sep)" of a strictly non-circular "(nc)" source at $\mu_1 = -1$ and a circular "(c)" source at $\mu_2 = -1 + \mathrm{sep}$ for $M = 8$, SNR = 10 dB, $N = 100$, $P^{(\mathrm{nc})} = 1$, and $P^{(\mathrm{c})} = 2$.

5. CONCLUSION

In this paper, we have developed the C-NC Standard ESPRIT and the C-NC Unitary ESPRIT algorithms designed to exploit the NC properties in a realistic scenario, where a mixture of circular and strictly non-circular signals is received. The number of circular and strictly non-circular signals is assumed known. The two proposed algorithms provide a lower estimation error and can resolve more sources than the traditional limit. Moreover, C-NC Unitary ESPRIT does not require a centro-symmetric array structure and can be implemented in an entirely real-valued fashion. As a main result, it has been shown via simulations that the estimation accuracy of the presented algorithms improves with an increasing the number of strictly non-circular signals among a fixed number of sources. Thereby, also the estimation accuracy of the circular signals is improved.

6. REFERENCES

[1] R. H. Roy and T. Kailath, "ESPRIT-estimation of signal parameters via rotational invariance techniques," *IEEE Transactions on Acoustics, Speech, and Signal Processing*, vol. 37, no. 7, pp. 984-995, July 1989.

[2] M. Haardt and J. A. Nossek, "Unitary ESPRIT: How to obtain increased estimation accuracy with a reduced computational burden," *IEEE Transactions on Signal Processing*, vol. 43, no. 5, pp. 1232-1242, May 1995.

[3] H. Abeida and J. P. Delmas, "MUSIC-like estimation of direction of arrival for noncircular sources," *IEEE Transactions on Signal Processing*, vol. 54, no. 7, pp. 2678-2690, July 2006.

[4] P. Chargé, Y. Wang, and J. Saillard, "A non-circular sources direction finding method using polynomial rooting," *Signal Processing*, vol. 81, no. 8, pp. 1765-1770, Aug. 2001.

[5] A. Zoubir, P. Chargé, and Y. Wang, "Non circular sources localization with ESPRIT," in *Proc. European Conference on Wireless Technology (ECWT 2003)*, Munich, Germany, Oct. 2003.

[6] M. Haardt and F. Roemer, "Enhancements of Unitary ESPRIT for non-circular sources," in *Proc. IEEE Int. Conf. on Acoust., Speech, and Sig. Proc. (ICASSP)*, Montreal, Canada, May 2004.

[7] J. Steinwandt, F. Roemer, M. Haardt, and G. Del Galdo, "R-dimensional ESPRIT-type algorithms for strictly second-order non-circular sources and their performance analysis," *IEEE Transactions on Signal Processing*, vol. 62, no. 18, pp. 4824–4838, Sep. 15, 2014.

[8] P. J. Schreier and L. L. Scharf, *Statistical Signal Processing of Complex-Valued Data: The Theory of Improper and Noncircular Signals*, Cambridge, U.K.: Cambridge Univ. Press, 2010.

[9] F. Gao, A. Nallanathan, and Y. Wang, "Improved MUSIC under the coexistence of both circular and noncircular sources," *IEEE Transactions on Signal Processing*, vol. 56, no. 7, pp. 30333038, July 2008.

[10] A. Liu, G. Liao, Q. Xu, and C. Zeng, "A circularity-based DOA estimation method under coexistence of noncircular and circular signals," in *Proc. IEEE Int. Conf. on Acoust., Speech, and Sig. Proc. (ICASSP)*, Kyoto, Japan, March 2012.

[11] A. Ferreol and P. Chevalier, "Higher order direction finding for arbitrary noncircular sources: The NC-2q-MUSIC algorithm," in *Proc. of the European Signal Processing Conference (EUSIPCO)*, Aalborg, Denmark, Aug. 2010.

[12] W. Si, T. Zhu, and M. Zhang, "A new approach for estimating the number of sources under the coexistence of circular and various noncircular sources," *Circuits, Systems and Signal Processing*, vol. 32, no. 6, pp. 3107-3119, Dec. 2013.

[13] M. Haardt, "Structured least squares to improve the performance of ESPRIT-type algorithms," *IEEE Transactions on Signal Processing*, vol. 45, pp. 792–799, Mar. 1997.